Journal of Materials Chemistry B

Accepted Manuscript

ROYAL SOCIETY OF CHEMISTRY

www.rsc.org/materialsB

Journal of Materials Chemistry B RSCPublishing

ARTICLE

Tough Protein/Carbon Nanotube Hybrid Fibers Comparable to Natural Spider Silks

Cite this: DOI: 10.1039/xoxxoooooox

Guangqiang Fang,[a]† Zhaokun Zheng,[a]† Jinrong Yao,[a] Min Chen,[b] Yuzhao Tang,[c] Jiajia Zhong,[c] Zeming Qi,[d] Zhao Li,[a] Zhengzhong Shao,[a] Xin Chen*[a]

Received 11th March 2015,
Accepted ooth April 2015

DOI: 10.1039/xoxxoooooox

www.rsc.org/

Animal silks, especially spider dragline silks, have the excellent portfolio of mechanical properties, but it is still a challenge to obtain the artificial silk fibers with the similar properties to the natural ones. In this paper, we show the possibility to extrude tough regenerated silk fiber by adding a few amount of commercially available functionalized multiwalled carbon nanotubes (less than 1%) though an environmentally friendly wet-spinning process reported in this laboratory previously. Most of the resulting regenerated silk fibers exhibit the breaking energy beyond 130 MJ/m^3 that is comparable to the spider dragline silks (~160 MJ/m^3). The most excellent performance of these fibers is the one showing the breaking stress of 0.42 GPa, breaking strain of 59%, and breaking energy of 186 MJ/m^3. In addition, we used several advanced characterization techniques, such as synchrotron radiation FTIR microspectroscopy and synchrotron radiation X-ray diffraction to reveal the toughening mechanism in such a protein/inorganic hybrid system. We believe our attempt to produce such tough protein-based hybrid fibers by using cheap, abundant, sustainable regenerated silkworm protein and commercially available functionalized carbon nanotubes, with a simplified industrial wet-spinning apparatus may open up a practical way for the industrial production of super-tough fiber materials.

Introduction

Bombyx mori silkworm silk has been applied in textile for several thousand years, but attracts a lot of attention in other fields, such as biotechnological and biomedical fields in recent few decades because of its acceptable mechanical strength, nontoxicity, good biocompatibility, and controllable biodegradability.[1-6] However, the figure-of-eight spinning behavior while silkworms produce silks naturally is the major drawback in terms of silkworm cocoon silk on its mechanical properties as it introduces defects in the fibers, making it is much inferior to spider dragline silks.[7] We have shown in our previous research that by directly force-reeling, we can get much stronger silkworm silk that has similar mechanical properties to spider dragline silks,[7] but obviously such a method is impossible for obtaining a large amount of strong silkworm silks. Alternatively but more practicable, many researchers devoted to find new methods to produce tough silk fibers from regenerated silk fibroin (RSF) solution, which has the abundant resource and is relatively cheap (even can make from waste silk materials, including unreelable dupion cocoons), by either wet-spinning or dry-spinning.[8-13] In this laboratory, we developed a wet-spinning method by extruding concentrated RSF solution into ammonium sulphate coagulation bath, followed by a continuous post-draw treatment.[14-16] Thus, we successfully obtained the RSF fibers with the breaking stress of 0.31–0.45 GPa, breaking stain of 28–37%, and breaking energy of 74.5–80.8 kJ/kg (equivalent to 101–109 MJ/m^3, if assuming the density of RSF fiber is the same as nature silkworm silk 1.35 g/m^3), which exceeds the toughness of natural *B. mori* silkworm cocoon silk (58[13]–70[4,17] MJ/m^3). Another useful method appeared in the literature to improve the mechanical properties of silk fiber is to disperse some nano- or functional materials in it. Recently, Zhang and his coworkers reported a simple and cheap method, which is to incorporate nanoanatase into silk protein, and produced a TiO_2 reinforced RSF fiber with breaking energy about 93 MJ/m^3.[18]

Carbon nanotube (CNT) is a fascinating material that is one atom thick layer of graphite rolled into a cylinder with 1 nm in diameter and several microns in length. Although it is light and flexible, it is hitherto the toughest material even known as it bears the elastic modulus of 1 TPa, the tensile strength of 100 GPa, and the breaking elongation of 30%.[19-21] Therefore, it is often used as the nanofillers for the preparation of light weight and high strength composites,[22-24] of course including for the enhancement of the mechanical properties of polymeric materials.[25-29] There are some reports on the combination of CNTs and silk fibroin to produce the reinforced RSF composite fibers by electrospinning,[30-32] but it is not a conventional "fiber", and its mechanical properties can hardly compare with natural silks (i.e., much worse). Considering we have a solid background on the wet-spinning of pure RSF fibers, we are eager to see if the RSF fibers will turn to be much tougher after we introduce CNTs in it.

Experimental

Preparation of RSF/CNT Spinning Dope: RSF aqueous solution was prepared from *B. mori* silkworm cocoons following a conventional procedure as described in our previous work.[14-16] In brief, raw *B. mori* silkworm silks were degummed twice with 0.5% (w/w) $NaHCO_3$ solution at 100 °C for 30 min and then washed with distilled water and allowed to air dry at room temperature. The degummed *B. mori* silk fibers were dissolved in 9.3 mol/L LiBr aqueous solution at 60 °C. After dialysis against deionized water in a Visking dialysis tube (MWCO: 10–12 kDa) for 3 days at room temperature, the solution was filtered and resulting SF solution was about 5% (w/w). Then the solution was concentrated by reverse dialysis with PEG aqueous solution to about 17% (w/w). One gram functionalized multiwalled CNTs (purchase from Nachen Science and Technology Development Co. Ltd., Beijing, China, with diameter of 8–15 nm and length of 5–30 μm) and 2 g sodium dodecyl sulphate (SDS) were added into 200 mL deionized water, followed by sonicating for 30 min to obtain a stable CNT suspension. Then the CNT suspension was added very carefully to concentrated RSF solution and stirred gently to make a homogeneous RSF/CNT spinning dope for wet-spinning. The RSF concentration in such spinning dope was set to 15%, and the mass ratio of CNT/RSF was 1/1000, 2/1000, 5/1000 and 10/1000, respectively.

Wet-spinning of RSF/CNT Hybrid Fibers: RSF/CNT hybrid fibers were produced by extruding RSF/CNT spinning dope into 35% (w/w) ammonium sulphate coagulation (60 °C) bath through a 200 μm spinneret in our custom-made wet-spinning device, as described in our previous work.[14-16] The take-up rate of the first roller was 60 r/min, equivalent to the spinning rate of was 9.4 m/min. The rotation rate of other three rollers was 18.8, 56.4, and 84.6 m/min, equivalent to the draw-down ratio of 2, 6, and 9, respectively. All resulting fibers were kept in coagulation bath for another 6 h and then immersed in deionized water to wash out ammonium sulphate. Throughout the text, we used label CNTa-bX to represent different samples, for example, sample CNT2-9X means CNT/RSF = 2/1000 and the draw-down ratio is 9.

Scanning Electron Microscopy (SEM): The surface and the cross-section of the RSF/CNT hybrid fibers were observed with a Tescan 5136MM SEM at 20 kV after sputtering with gold. The cross-section of the hybrid fibers was obtained by fracturing them perpendicular to the fiber axis under liquid nitrogen. The areas of the RSF/CNT hybrid fibers were calculated by software Atlas 2.9.9.9, provided with the SEM. For each kind of RSF/CNT hybrid fiber, the average area was obtained from at least 12 samples.

Mechanical Testing: The mechanical properties of RSF/CNT hybrid fibers were tested with an Instron 5565 mechanical testing instrument (at 25 °C and 45% R.H.; gauge length: 30 mm; cross-head speed: 15 mm/min) with a load cell of 2.5 N. At least 12 replicates from individual fibers were used for mechanical testing. For each hybrid fiber sample, we cut them into two part, one for mechanical testing and one for measuring the area of cross-section by SEM image mentioned above.

Raman Spectroscopy: Raman dichroism spectra of RSF/CNT hybrid fibers were collected with a Renishaw inVia Reflex Raman spectrometer, using the 785 nm wavelength of a He-Ne laser with the energy of 6 mW. Single RSF/CNT hybrid fibers were aligned perpendicular or parallel to the direction of the laser beam. At least 6 individual fibers were used in each Raman measurement.

Synchrotron Radiation FTIR Spectroscopy: The preliminary experiment was carried out at Beamline U4 at the National Synchrotron Radiation Laboratory (NSRL). The description of Beamline U4 can be found in our previous paper.[33] The data collection were mainly performed at Beamline BL01B1 at the National Center for Protein Science • Shanghai (NCPSS) in Shanghai Synchrotron Radiation Facility (SSRF). The infrared beamline at NCPSS-SSRF is extracted from a conventional bending magnet with an acceptance angle of 40(H)×20(V) $mrad^2$. The endstation is equipped with an FTIR spectrometer (Nicolet 6700) with a KBr beamsplitter and various detectors (in this study, we used a liquid nitrogen cooled MCT detector) coupled with a Nicolet Continuμm microscope with a 36x objective. For each measurement, 256 interferograms were coadded and transformed employed a Genzel-Happ apodization function to yield spectra with a nominal resolution of 4 cm^{-1}. Deconvolution of amide III bands was carried out using PeakFit 4.12 according to the method reported in our previous work.[33,34]

Synchrotron Radiation Wide Angle X-ray Diffraction (WAXD): The experiments were performed at Beamline BL16B1 at SSRF with a wavelength of 0.124 nm. RSF/CNT hybrid fiber bundles were glued to a sample holder. The detector-to-sample distance was calibrated to 115 mm. A diffraction pattern of background was collected prior to the measurement of each sample. Date analysis was carried out by FIT2D (v 12.077) software. Deconvolution of 1D WAXD profile was carried out using PeakFit 4.12. During the deconvolution process, the numbers and positions of peaks were fixed by using the data reported in the literature.[35] A Gaussian model was selected for the band shape, and the bandwidth was automatically adjusted by the software.[36] The Bragg reflections were separated from the broad short-range order background to estimate the crystallinity (*X*c) of the fiber, which is measured as a ratio of crystalline area to total area. The crystallite size (L) were determined by Scherrer's equation.[37] The reflection profile of (200) lattice plane was azimuthally integrated with a region of 180 ° from 2D WAXD patterns at d-spacing of 4.3Å, and the traditional orientation degree Π was calculated from FWHM (full width at half-maximum) of the corresponding peak as follows.

$$\Pi = \left(1 - \frac{FWHM}{180}\right) \times 100\%$$

Results and Discussion

Spinning of RSF/CNT hybrid Fibers and Their Mechanical Properties

We used the same spinning method for the preparation of RSF/CNT hybrid fibers as the pristine RSF fibers,[14-16] and the spinning parameters we chose are also similar to the optimal conditions when obtaining pristine RSF fibers after some preliminary experiments. That is, the final silk fibroin concentration in the spinning dope is 15% (w/w), the spinning rate is 60 r/min (equivalent to 9.4 m/min), and the concentration and the temperature of ammonium sulphate coagulation is 35% (w/w) and 60 °C, respectively. Besides the determination of spinning parameters, another key issue before the spinning is to obtain a stable and homogeneous RSF/CNT spinning dope.

First, we used SDS to help the dispersion of functionalized multiwalled CNTs in de-ionized water. Then, we added such SDS-stabilized CNTs dispersion into RSF aqueous solution to form a uniform RSF/CNT solution (Fig. S1). Such a RSF/CNT solution is stable and without gelation or precipitation for at least 2 days that is long enough for wet-spinning. We attribute such a phenomenon to the amphiphilic natural of silk fibroin and the surfactant SDS we added. They may coat or attach on the surface of CNTs, allowing them stably dispersed in RSF solution without any gelation or precipitation.[38]

Fig. 1A shows the appearance of our RSF/CNT hybrid fiber, which is fairly uniform and highly lustrous. The black color clearly indicates the presence of CNTs in the fiber. During the spinning, we selected four different CNT/RSF mass ratio (i.e., 1/1000, 2/1000, 5/1000 and 10/1000), and performed a three stage post-draw (i.e., the draw-down ratio is 2, 6, and 9) as reported previously.[16] It should be mentioned that in our former experiments, the pristine RSF fibers only stand for 6 times postdraw,[14,15] unless adding calcium ions in the spinning dope.[16] Here we find by incorporating CNTs, it can easily subject to 9 times postdraw without the addition of calcium ions. Fig. 1B is the SEM image of a typical RSF/CNT hybrid fiber, sample CNT2-9X. It shows a smooth surface and a dense cross-section, which are both homogeneous. There is no obvious aggregation of CNTs found in either surface or cross-section, which could be an evidence of the well-dispersion of CNTs in silk fibroin matrix. The cross-section is tabular that is similar to the wild silkworm silks,[4] with the long axis of 25-30 μm and the short axis of about 10 μm.

Fig. 1C demonstrates the representative stress-strain curves for RSF/CNT hybrid fibers with different draw-down ratio. Obviously, the as-spun fiber is very weak and brittle (curve a).

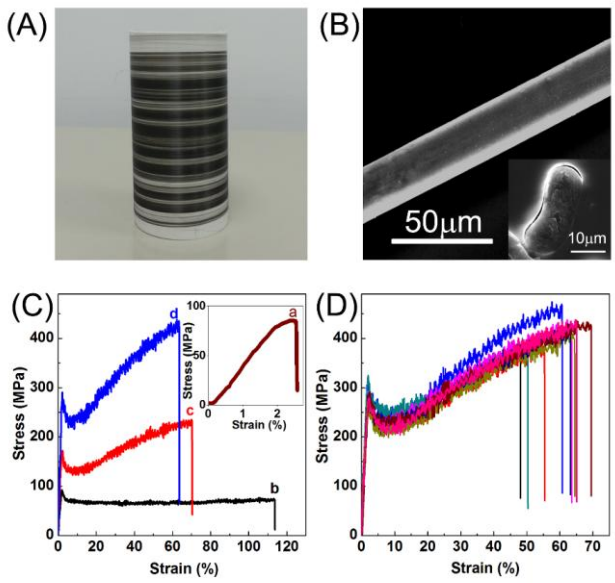

Fig. 1 (A) Digital photo of RSF/CNT hybrid fiber; (B) SEM images of the surface and the cross-section (inset) of CNT2-9X silk fiber; (C) Stress-strain curves of RSF/CNT hybrid fibers with different draw ratio (a: CNT2-1X, b: CNT2-2X, c: CNT2-6X, d: CNT2-9X); (D) Stress-strain curves of different CNT2-9X fibers. Fig. 1. (A) Digital photo of RSF/CNT hybrid fiber; (B) SEM images of the surface and the cross-section (inset) of CNT2-9X silk fiber; (C) Stress-strain curves of RSF/CNT hybrid fibers with different draw ratio (a: CNT2-1X, b: CNT2-2X, c: CNT2-6X, d: CNT2-9X); (D) Stress-strain curves of different CNT2-9X fibers.

Although the fiber with draw-ratio of 2 shows a large breaking strain (about 110%), its strength is still fairly low (<100 MPa). However, with the further increase in draw-down ratio to 6 and 9, the shape of the strain-strain curves begins to appear like a tough material. We can find after a yield point at about 2% of strain, the stress shows a tensile hardening trend, which is more similar to the spider dragline silk than that of the silkworm silk.[7] In addition, the tensile behavior of these RSF/CNT hybrid fibers is highly repetitively, as the stress-strain curves from different samples are almost identical (Fig. 1D).

Table 1 summarizes the mechanical properties of the RSR/CNT hybrid fibers. It clearly shows that all of these hybrid fibers (CNT/RSF ratio from 1/1000 to 1/100, draw-down ratio of 6 or 9) exhibit excellent toughness, that is, the breaking energy is about 130-160 MJ/m^3, which is much larger than most of the reported artificial silk fibers[11,18,39] and comparable to spider dragline silks (the mechanical properties of *Nephila edulis* spider dragline silk measured by the same testing machine and condition in this work is included in Table 1 for comparison). These fibers can be divided into two catalogs based on the draw-down ratio. For the fibers obtained from draw-down ratio of 6, the breaking stresses, breaking strains, and breaking energies are 0.20–0.23 GPa, 70–77%, and 107–137 MJ/m^3; while for those from draw-down ratio of 9, these data are 0.34–0.42 GPa, 52–59%, and 150–186 MJ/m^3, respectively. It is not surprising because many previous works also find that the high post-draw ratio results in larger breaking stress and energy but lower breaking strain. Different from the draw-down ratio, the CNT content in hybrid fiber seems have little effect on the mechanical properties at the amount we added in this research. Among them, the CNT2-9X hybrid fiber has the best performance: the breaking stress, breaking strain, and breaking energy is 0.42±0.03 GPa, 59±7%, and 186±30 MJ/m^3, which is exceed the typical value of spider dragline silk 160 MJ/m^3, respectively.[4,17] In the meantime, the CNT10-9X hybrid fiber seems to be relatively weak, and this may because the relatively high CNT content is not favorable to form uniform structure of the fiber, especially when subject to high ratio of post-draw. Overall, we find the greatly improvement on the toughness of such a RSF fiber is mainly attributed to the significant increase of extensibility because the breaking stress is almost the same as natural silkworm cocoon silk and pristine RSF fiber.[14-16]

Characterizations of RSF/CNT hybrid Fibers

From the data shown above, it is no doubt that we can produce tough RSF fibers only by incorporating a few amount of CNTs (less than 1%). In order to reveal the possible reasons for such an improvement or enhancement, we tried to characterize the structure of RSF/CNT hybrid fibers to determine several major aspects related to the mechanical properties of silk fiber, i.e., the proportion of ordered phase (β-sheet or silk II content), the size of β-sheet nanocrystals, and the orientation of the molecular chain in the fiber.

In our previous work, we have developed a practical method to determine the β-sheet content quantitatively in single silk fiber with the synchrotron radiation FTIR microspectroscopy.[33,34] Fig. 2A shows a typical synchrotron radiation FTIR spectrum of the RSF/CNT hybrid fiber, in which the major characteristic adsorption bands of silk fibroin are well resolved. According to our previous method, the β-sheet content of silk fibroin in the fibers can be obtained from the deconvolution of amide III band in the FTIR spectra (Fig.

2B and Fig. S2). As no adsorption band of CNT is found in this region, so we can easily get the β-sheet in the RSF/CNT hybrid fibers with different draw-down ratio, and the results are listed in Table 2. Beyond our expectation, the β-sheet contents in the hybrid fibers are quite large, the value of as-spun fiber and slight post-draw fiber (CNT2-1X and CNT2-2X) is close to the value of natural silkworm cocoon silk (about 28%[33]), and the one has the highest draw-down ratio (CNT2-9X) even reaches 33.7%. For comparison, we used the same method to determine the β-sheet content of pristine RSF fibers with same spinning parameters. The results indicate that the β-sheet content in pristine RSF fibers is lower than the corresponding RSF/CNT hybrid fibers. For instance, the value of RSF fiber obtained from draw-down ratio of 6 is 25.9±0.6% (unpublished data), which is obviously less than that of CNT2-6X fiber reported here (29.6±0.5%). Therefore, we have the reason to assume that the CNTs we added may serve as a nucleating agent to promote the formation of β-sheet crystals.

Table 1. Mechanical properties of RSF/CNT hybrid fibers

Samples	Breaking Stress (GPa)	Breaking Strain (%)	Breaking Energy (MJ/m^3)	Breaking Energy (kJ/kg)
CNT1-6X	0.23±0.04	71±18	130±31	96±23
CNT1-9X	0.39±0.01	52±7	162±29	120±21
CNT2-6X	0.23±0.02	72±14	126±31	93±23
CNT2-9X	0.42±0.03	59±7	186±30	138±22
CNT5-6X	0.20±0.02	70±16	107±30	79±22
CNT5-9X	0.41±0.02	56±3	167±12	124±9
CNT10-6X	0.22±0.01	77±11	137±23	101±17
CNT10-9X	0.34±0.02	56±6	150±21	111±16
Spider dragline silk	1.01±0.15	37±9	146±32	—
Pristine RSF fibers[14-16]	0.31–0.45	28–37	101–109	74–81

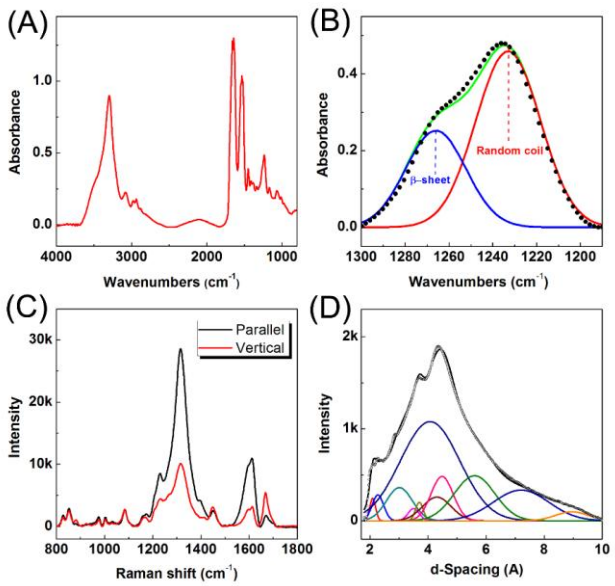

Fig. 2 Synchrotron radiation FTIR spectrum (A) and deconvolution of the corresponding amide III band (B), Raman dichroism spectra (C), and synchrotron radiation WAXD 1D profile of CNT2-9X fiber.

Raman dichroism has been widely used to determine the molecular orientation in polymer fibers, including silk fibers.[15,40-45] The intensity difference in Raman spectra at different beam direction (parallel or perpendicular) is a label to estimate the molecular alignment along the fiber axis. Fig. 2C shows the typical Raman dichroism spectra of RSF/CNT hybrid fibers. We can find two distinct adsorption band of CNTs at about 1610 cm^{-1} (G band) and 1310 cm^{-1} (D band).[46,47] We also can find the characteristic silk fibroin amide I band at about 1667 cm^{-1}, however, the amide III band (1230 cm^{-1}) becomes a shoulder peak of the strong CNT D band and is not well distinguishable. It is very interesting that the characteristic Raman bands of CNTs also have dichroism, so we can use both the intensity difference of silk fibroin amide I band (1667 cm^{-1}) and CNT G band (1610 cm^{-1}) to monitor the molecular orientation of protein backbone as well as the CNTs along the fiber axis. Fig. S3 shows the Raman spectra of RSF/CNT hybrid fibers with CNT/RSF ratio of 2/1000 at different draw-down ratio, and Table 2 presents the intensity ratios of the silk fibroin amide I band $I(1667)_v/I(1667)_p$ as well as the CNT G band $I(1610)_p/I(1610)_v$. The $I(1667)_v/I(1667)_p$ ratio of amide I band increases progressively with the draw-down ratio increases from 1 to 9, which is consistent with the results we reported previously for pristine RSF fibers.[15] However, the addition of CNTs seems not improve the orientation of silk fibroin molecular chains (for instance, the $I(1667)_v/I(1667)_p$ ratio of pristine RSF fiber with draw-down ratio of 6 is also around 2.7[15]), and the highest value

Table 2. Characterization of β-sheet content and molecular orientation in RSF/CNT hybrid fibers with synchrotron radiation FTIR and Raman spectroscopy

Sample	β-sheet content (%)	$I(1667)_v/I(1667)_p$	$I(1610)_p/I(1610)_v$
CNT2-1X	28.7±0.5	1.2	2.3
CNT2-2X	28.8±0.4	1.4	2.6
CNT2-6X	29.6±0.5	2.7	3.2
CNT2-9X	33.7±0.4	2.9	3.4

in RSF/CNT hybrid fiber is still low than natural cocoon silk (about 3.1). In the meantime, the $I(1610)_p/I(1610)_v$ ratio of CNT G band also increases with the increase in draw-down ratio, which not only indicates CNTs align along the fiber axis, but also shows their orientation degree is improved during the post-draw.

Apart from FTIR and Raman spectroscopy, wide-angle X-ray diffraction (WAXD) is another powerful technique to determine the structures of silk fibers.[48,49] It can provide complementary information on the crystallinity (closely related to β-sheet content in silk fiber) and the orientation degree of the crystalline structures.[50,51] Similar to synchrotron radiation FTIR spectroscopy, we also used synchrotron radiation X-ray beam to perform the WAXD experiment because the small size of our samples. Fig. 3 shows the typical 2D WAXD patterns of RSF/CNT hybrid fibers. All samples demonstrate a clear diffraction pattern, indicating the existence of certain crystallinity. However, the as-spun fiber (CNT2-1X) only shows diffraction rings, reflecting a very poor orientation of the sample. When the draw-down ratio is from 2 to 9, the diffraction arcs are more and more clear in the meridian direction, which is an evidence of the increase in preferential orientation along the fiber axis. In addition, we can find an increase of the diffraction intensity with the increase in draw-down ratio, which implies the increase of crystallinity. Fig. 2D and Fig. S4 shows the 1D WAXD patterns derived from the 2D patterns, in which some typical β-sheet characteristic peaks with crystalline spacing of 4.3/4.5, 3.5/3.7, and 2.09/2.26Å corresponding to the reflection of (200)/(020), (002)/(021), and (420)/(040)[29,52-54] facets can be found. According to the literature,[16] we calculated the crystallinity and the crystallite size in different hybrid fiber samples, and the results are listed in Table 3. The data of crystallinity is consistent with the FTIR results (β-sheet content) very well. Firstly, it is expectable that the crystallinity increases with the draw-down ratio increases from 1 to 9. Secondly, the crystallinity of the hybrid fiber with the draw-down ratio 6 and 9 is larger than that of natural cocoon silk. Thirdly, the crystallinity of the hybrid fiber is larger than that of pristine RSF fiber with the same draw-down ratio, for example, it is only 51.3% for pristine RSF fiber with the draw-down ratio of 6 (unpublished data), and here is 54.1%. In the meantime, we find the crystallite size in the hybrid fibers decreases with the increase in the draw-down ratio, which also can be seen from RSF/TiO_2 hybrid fibers by dry-spinning process[13]. Actually, this phenomenon is found in the natural spinning process *Nephila pilipes* spider silk[37] and *B. mori* silkworm silk.[49] The appearance of the smaller crystallites with the high draw-down ratio may result from the reduction of the defects in the crystallites,[16] as when the as-spun fiber subjects to more post-draw treatment, the molecular chain may have more chance to rearrange, forming a relatively "perfect" β-sheet crystals.

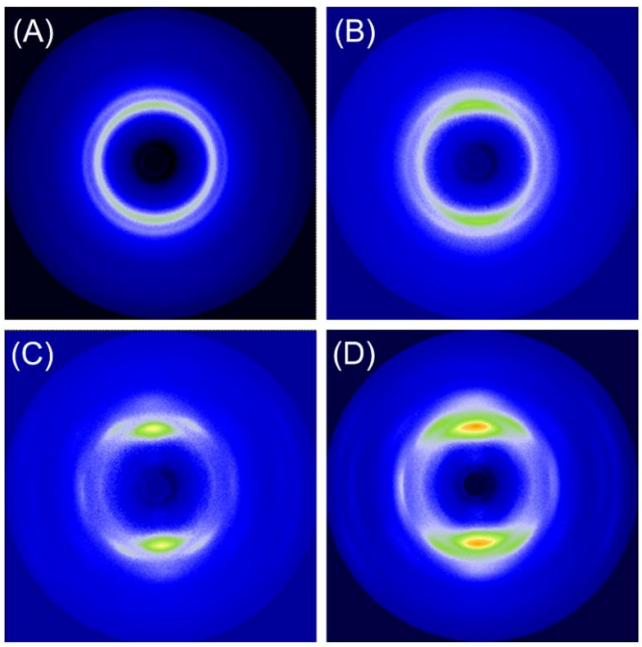

Fig. 3 Synchrotron radiation 2D WAXD patterns of RSD/CNT hybrid fibers. (A) CNT2-1X; (B) CNT2-2X; (C) CNT2-6X; (D) CNT2-9X.

To investigate the orientation degree of the molecular chains in RSF/CNT hybrid fibers, the peak intensity of (200) lattice plane from 2D WAXD diffraction pattern is plotted versus the azimuthal angle to illustrate the β-sheet orientation in the fibers.[35] It is shown in Table 3 that with the increase in draw-down ratio, the orientation degree also increases. Such a result accords well with the Raman analysis, which proves that the post-draw is favorable to improve the alignment of the molecular chains along the fiber axis. Moreover, similar to the Raman dichroism data again, the results from WAXD prove the addition of CNTs does not significantly improve the orientation of silk fibroin molecular chains, for instance, the orientation degree of pristine RSF fiber with the draw-down ratio of 6 is 82.3% (unpublished data), and here is 85.2%. The orientation degree of CNT2-9X fiber is still lower than that of natural cocoon silks, implying that there is still some distance between our artificial spinning method and the natural evolutionary one.

Discussions on the Possible Toughening Mechanism

Based on the outstanding properties and the corresponding structural analysis of the RSF/CNT hybrid fibers shown above, we propose the possible toughening mechanism of CNTs to RSF fibers. First, CNTs may help the conformation conversion of silk fibroin (i.e., β-sheet formation) or crystallization during the spinning process. They may serve as crystal nucleus to form more β-sheet structures and speed up the crystallization process. Therefore, the β-sheet contents or crystallinities of those RSF/CNT hybrid fibers at draw-down ratio of 6 or 9 are higher (Table 2 and 3), but the crystallite sizes are smaller than that of natural cocoon silks (Table 3). It is commonly accepted that large β-sheet content or high crystallinity is favorable to the mechanical strength of the silk fiber, so considering the β-sheet content (30-33% to 28%) or the crystallinity (54-56% to 52%) of our RSF/CNT hybrid fibers to natural cocoon silks, the addition of CNTs is favorable to improve the mechanical properties of the resulting RSF fibers. In the meantime, the crystallite sizes of RSF/CNT hybrid fibers with high draw-down ratio (6 or 9) are smaller than the natural cocoon silk. From the molecular dynamics simulation, it is concluded that β-sheet nanocrystals confined to a few nanometers have high stiffness, strength, and mechanical toughness than larger nanocrystals. Smaller β-sheet nanocrystals provide a greater stiffness and fracture resistance, as they are predominantly loaded in uniform shear, which leads to cooperative rupture of hydrogen bonds and stick-slip energy dissipation mechanisms.[55] In addition, the smaller crystallite size in spider dragline silks than that in *B. mori* silkworm silks is also considered as a reason for the better mechanical properties of spider dragline silks than silkworm silks.[56]

Another reason we assume, which we think is more important, is CNTs may act as "bridges" or "crosslinkers" to bind silk fibroin macromolecular chains together though CNTs seem have no effect to improve the orientation of these polypeptide chains. We know the functionalized CNTs we used have functional groups, mainly carboxyl groups, which can have strong interactions with the polar amino acid residues on the protein chains. In addition, there are also significant van der Waals interactions between CNTs and protein chains, as silk fibroin also have large amount of nonpolar amino acid residues, which is similar to the situation reported by Hamedi and his coworkers in the nanofibrillated cellulose/CNTs composites.[57] Therefore, these interactions maintain the connections between the polypeptide chains when the RSF/CNT hybrid fibers subjected to stretch. Meanwhile, it is well accepted that stress transfer effect of CNTs arising from their huge surface area and more uniform stress distribution can minimize the presence of stress concentration centers.[58] That is, during the stretching, while the protein chains become more and more extended, they may slip along the axis of CNTs (both silk fibroin chains and CNTs are paralleled aligned along the fiber axis), keeping the interactions existed and not breaking down. Raman dichroism spectra (Fig. 2c) indicate that CNTs in the hybrid fiber are also well-oriented, which makes such an assumption reasonable. Of course, the strongest evidence to support this assumption is the strain-stress curves of RSF/CNT hybrid fibers (Fig. 1c). They have much larger breaking strain than natural silkworm silks or RSF fibers. In addition, the change of stress after the yield point is almost linearly to the strain, which seems have less entanglement between the molecular chains, but we cannot imagine that less than 1% of CNTs can trigger the disentanglement of silk fibroin chains in the spinning dope. Thus as a result, the increased extensibility at a considerable high stress level makes the RSF/CNT hybrid fibers rather tough. Although their breaking stresses are still quite lower than spider dragline silks, profiting from the large breaking strain, the RSF/CNT hybrid fibers own the similar toughness to the spider dragline silks.

Table 3. Crystallinity and crystal size in RSF/CNT hybrid fibers

Sample	Crystallinity (%)	Crystallite sizes (nm)			Orientation degree (%)
		L_a	L_b	L_c	
CNT2-1X	47.2	3.9	5.0	9.2	--
CNT2-2X	53.3	3.4	4.7	8.3	76.3
CNT2-6X	54.1	2.9	3.9	6.9	85.2
CNT2-9X	56.0	2.8	3.7	6.4	89.3
Natural cocoon silk	52.4	3.4	3.8	8.8	92.8

Conclusions

We successfully prepared tough RSF/CNT hybrid fibers by using cheap abundant, and sustainable regenerated silkworm protein and commercially available functionalized CNTs, with a simplified industrial wet-spinning apparatus. By adding 0.1–1% of CNTs, most of the resulting RSF fibers exhibit the breaking energy beyond 130 MJ/m^3 that is comparable to the spider dragline silks. The most excellent performance of these RSF/CNT hybrid fibers is CNT2-9X, which shows the breaking stress of 0.42 GPa, breaking strain of 59%, and breaking energy of 186 MJ/m^3. If we choose different post draw-down ratio (6 or 9), we can obtain two class of hybrid fiber, one has relatively low breaking stress and large breaking strain (draw-down ratio of 6), and the other has high breaking stress but relatively small breaking strain (draw-down ratio of 9). As these two kinds of hybrid fiber have the similar breaking energy, and the small amount of CNTs addition (less than 1%) will not affect the protein nature of these fibers, so we have the opportunity to select suitable fibers according to the requirement of different application. In the meantime, we used several advanced analytical methods, including synchrotron radiation FTIR spectroscopy, synchrotron radiation WAXD, and Raman dichroism spectroscopy to determine the structure of RSF/CNT hybrid fibers. The results suggest that the addition of CNT is favorable to the formation of β-sheet structure (increase of crystallinity) and decrease of crystallite size, which helps us to propose the possible toughening mechanism for the CNTs to the RSF fibers.

Acknowledgements

This work is supported by the National Natural Science Foundation of China (Nos. 10979022, 20974025, and 21034003). We thank Dr. Feng Tian, Dr. Fenggang Bian at SSRF, and Dr. Yuhong Yang at Fudan University for their valuable suggestions and discussions.

Notes and references

[a]State Key Laboratory of Molecular Engineering of Polymers, Collaborative Innovation Center of Polymers and Polymer Composite Materials, Department of Macromolecular Science, Laboratory of Advanced Materials, Fudan University, Shanghai, 200433, People's Republic of China. E-mail: chenx@fudan.edu.cn

[b]Shanghai Synchrotron Radiation Facility, Shanghai Institute of Applied Physics, Chinese Academy of Sciences, Shanghai, 201203, People's Republic of China.

[c]National Center for Protein Science • Shanghai, Institute of Biochemistry and Cell Biology, Shanghai Institutes for Biological Sciences, Chinese Academy of Sciences, Shanghai, 201210, People's Republic of China.

[d]National Synchrotron Radiation Laboratory, University of Science and Technology of China, Hefei, 230029, People's Republic of China.

†G. Q. Fang and Z. K. Zheng contributed equally to this work.

Electronic Supplementary Information (ESI) available: Photograph of the homogenous RSF/CNT spinning dope solution; deconvolution of amide III band in synchrotron radiation FTIR spectra of RSF/CNT hybrid fibers; Raman dichroism spectra of RSF/CNT hybrid fibers; synchrotron

radiation WAXD 1D profiles of RSF/CNT hybrid fibers. See DOI: 10.1039/b000000x/

1 D. H. Kim, J. Viventi, J. J. Amsden, J. L. Xiao, L. Vigeland, Y. S. Kim, J. A. Blanco, B. Panilaitis, E. S. Frechette, D. Contreras, D. L. Kaplan, F. G. Omenetto, Y. G. Huang, K. C. Hwang, M. R. Zakin, B. Litt and J. A. Rogers, *Nat. Mater.*, 2010, **9**, 511-517.
2 S. Talukdar and S. C. Kundu, *Adv. Funct. Mater.*, 2012, **22**, 4778-4788.
3 E. M. Pritchard, T. Valentin, B. Panilaitis, F. Omenetto and D. L. Kaplan, *Adv. Funct. Mater*., 2013, **23**, 854-861.
4 F. G. Omenetto and D. L. Kaplan, *Science*, 2010, **329**, 528-531.
5 A. M. Hopkins, L. De Laporte, F. Tortelli, E. Spedden, C. Staii, T. J. Atherton, J. A. Hubbell and D. L. Kaplan, *Adv. Funct. Mater.*, 2013, **23**, 5140-5149.
6 H. Tao, D. L. Kaplan and F. G. Omenetto, *Advanced materials*, 2012, **24**, 2824-2837.
7 Z. Z. Shao and F. Vollrath, *Nature*, 2002, **418**, 741-741.
8 S. W. Ha, A. E. Tonelli and S. M. Hudson, *Biomacromolecules*, 2005, **6**, 1722-1731.
9 O. Liivak, A. Blye, N. Shah and L. W. Jelinski, *Macromolecules*, 1998, **31**, 2947-2951.
10 C. H. Zhao, J. M. Yao, H. Masuda, R. Kishore and T. Asakura, *Biopolymers*, 2003, **69**, 253-259.
11 J. M. Yao, H. Masuda, C. H. Zhao and T. Asakura, *Macromolecules*, 2002, **35**, 6-9.
12 K. A. Trabbic and P. Yager, *Macromolecules*, 1998, **31**, 462-471.
13 M. J. Sun, Y. P. Zhang, Y. M. Zhao, H. L. Shao and X. C. Hu, *J. Mater. Chem.*, 2012, **22**, 18372-18379.
14 J. P. Yan, G. Q. Zhou, D. P. Knight, Z. Z. Shao and X. Chen, *Biomacromolecules*, 2010, **11**, 1-5.
15 G. Q. Zhou, Z. Z. Shao, D. P. Knight, J. P. Yan and X. Chen, *Adv. Mater*., 2009, 21, 366-370.
16 H. Zhou, Z. Z. Shao and X. Chen, *Chin. J. Polym. Sci.*, 2014, **32**, 29-34.
17 S. Kubik, *Angew. Chem.-Int. Edit.*, 2002, **41**, 2721-2723.
18 H. Pan, Y. P. Zhang, H. L. Shao, X. C. Hu, X. H. Li, F. Tian and J. Wang, *J. Mat. Chem. B*, 2014, **2**, 1408-1414.
19 J. P. Lu, *Phys. Rev. Lett.*, 1997, **79**, 1297-1300.
20 B. Peng, M. Locascio, P. Zapol, S. Y. Li, S. L. Mielke, G. C. Schatz and H. D. Espinosa, *Nat. Nanotechnol.*, 2008, **3**, 626-631.
21 M. F. Yu, O. Lourie, M. J. Dyer, K. Moloni, T. F. Kelly and R. S. Ruoff, *Science*, 2000, **287**, 637-640.
22 S. Kim, J. Byun, S. Choi, D. Kim, T. Kim, S. Chung and Y. Hong, *Adv. Mater.*, 2014, **26**, 3094-3099.
23 C. J. Shearer, A. Cherevan and D. Eder, *Adv. Mater.*, 2014, **26**, 2295-2318.
24 X. M. Sun, H. Sun, H. P. Li and H. S. Peng, *Adv. Mater.*, 2013, **25**, 5153-5176.
25 A. B. Dalton, S. Collins, E. Munoz, J. M. Razal, V. H. Ebron, J. P. Ferraris, J. N. Coleman, B. G. Kim and R. H. Baughman, *Nature*, 2003, **423**, 703-703.
26 P. Miaudet, S. Badaire, M. Maugey, A. Derre, V. Pichot, P. Launois, P. Poulin and C. Zakri, *Nano Lett.*, 2005, **5**, 2212-2215.
27 M. Naraghi, T. Filleter, A. Moravsky, M. Locascio, R. O. Loutfy and H. D. Espinosa, *Acs Nano*, 2010, **4**, 6463-6476.
28 K. Saeed and S. Y. Park, *J. Polym. Res.*, 2010, **17**, 535-540.
29 R. Sen, B. Zhao, D. Perea, M. E. Itkis, H. Hu, J. Love, E. Bekyarova and R. C. Haddon, *Nano Lett.*, 2004, **4**, 459-464.
30 K. Wei, J. H. Xia, B. S. Kim and I. S. Kim, *J. Polym. Res.*, 2011, **18**, 579-585.
31 M. Kang, P. Chen and H. J. Jin, *Curr. Appl. Phys.*, 2009, **9**, S95-S97.
32 H. Pan, Y. P. Zhang, Y. C. Hang, H. L. Shao, X. C. Hu, Y. M. Xu and C. Feng, *Biomacromolecules*, 2012, **13**, 2859-2867.
33 S. J. Ling, Z. M. Qi, D. P. Knight, Z. Z. Shao and X. Chen, *Biomacromolecules*, 2011, **12**, 3344-3349.
34 S. J. Ling, Z. M. Qi, D. P. Knight, Y. F. Huang, L. Huang, H. Zhou, Z. Z. Shao and X. Chen, *Biomacromolecules*, 2013, **14**, 1885-1892.
35 J. Luo, L. L. Zhang, Q. F. Peng, M. J. Sun, Y. P. Zhang, H. L. Shao and X. C. Hu, Int. J. Biol. Macromol., 2014, **66**, 319-324.
36 A. Martel, M. Burghammer, R. J. Davies and C. Riekel, *Biomacromolecules*, 2007, **8**, 3548-3556.
37 N. Du, X. Y. Liu, J. Narayanan, L. A. Li, M. L. M. Lim and D. Q. Li, *Biophys. J.*, 2006, **91**, 4528-4535.
38 J. Ayutsede, M. Gandhi, S. Sukigara, H. H. Ye, C. M. Hsu, Y. Gogotsi and F. Ko, *Biomacromolecules*, 2006, **7**, 208-214.
39 S. W. Ha, Y. H. Park and S. M. Hudson, *Biomacromolecules*, 2003, **4**, 488-496.
40 Z.Z. Shao, F. Vollrath, J. Sirichaisit and R. J. Young, *Polymer*, 1999, **40**, 2493-2500.
41 Z. Z. Shao, R. J. Young and F. Vollrath, *Int. J. Biol. Macromol.*, 1999, **24**, 295-300.
42 J. Sirichaisit, V. L. Brookes, R. J. Young and F. Vollrath, *Biomacromolecules*, 2003, **4**, 387-394.
43 V. Sereda and I. K. Lednev, *J. Raman Spectrosc.*, 2014, **45**, 665-671.
44 C. P. Yuan, J. J. Wang, G. M. Chen, J. H. Zhang and J. P. Yang, *Soft Matter*, 2011, **7**, 4039-4044.
45 M. S. Park, Y. S. Wong, J. O. Park, S. S. Venkatraman and M. Srinivasarao, *Macromolecules*, 2011, **44**, 2120-2131.
46 K. K. Kim, J. S. Park, S. J. Kim, H. Z. Geng, K. H. An, C. M. Yang, K. Sato, R. Saito and Y. H. Lee, *Phys. Rev. B*, 2007, **76**.
47 T. M. Wu, Y. W. Lin and C. S. Liao, *Carbon*, 2005, **43**, 734-740.
48 X. D. Liu and W. Ruland, *Macromolecules*, 1993, **26**, 3030-3036.
49 L. F. Drummy, B. L. Farmer and R. R. Naik, *Soft Matter*, 2007, **3**, 877-882.
50 D. M. Phillips, L. F. Drummy, R. R. Naik, H. C. De Long, D. M. Fox, P. C. Trulove and R. A. Mantz, *J. Mater. Chem.*, 2005, **15**, 4206-4208.
51 S. Sampath, T. Isdebski, J. E. Jenkins, J. V. Ayon, R. W. Henning, J. Orgel, O. Antipoa and J. L. Yarger, *Soft Matter*, 2012, **8**, 6713-6722.
52 R. E. Marsh, R. B. Corey and L. Pauling, *Biochim. Biophys. Acta*, 1955, 16, 1-34.
53 R. E. Marsh, R. B. Corey and L. Pauling, *Acta Crystallogr.*, 1955, 8, 62-62.
54 Y. Takahashi, M. Gehoh and K. Yuzuriha, *Int. J. Biol. Macromol.*, 1999, **24**, 127-138.
55 S. Keten, Z. P. Xu, B. Ihle and M. J. Buehler, *Nat. Mater.*, 2010, **9**, 359-367.
56 A. Nova, S. Keten, N. M. Pugno, A. Redaelli and M. J. Buehler, *Nano Lett.*, 2010, **10**, 2626-2634.

57 M. M. Hamedi, A. Hajian, A. B. Fall, K. Hakansson, M. Salajkova, F. Lundell, L. Wagberg and L. A. Berglund, *Acs Nano*, 2014, **8**, 2467-2476.
58 Y. Hou, J. Tang, H. B. Zhang, C. Qian, Y. Y. Feng and J. Liu, *Acs Nano*, 2009, **3**, 1057-1062.

